Nuclear Instruments and Methods in Physics Research A 791 (2015) 58–64

Contents lists available at ScienceDirect

Nuclear Instruments and Methods in Physics Research A

journal homepage: www.elsevier.com/locate/nima

First use of single-crystal diamonds as fission-fragment detector

M.O. Frégeau [a], S. Oberstedt [a,*], T. Bryś [a], Th. Gamboni [a], W. Geerts [a], F.-J. Hambsch [a], A. Oberstedt [b,c], M. Vidali [a]

[a] European Commission, DG Joint Research Centre (IRMM), B-2440 Geel, Belgium
[b] OSSOLUTIONS Consulting, S-70353 Örebro, Sweden
[c] Fundamental Physics, Chalmers University of Technology, S-41296 Göteborg, Sweden

ARTICLE INFO

Article history:
Received 9 January 2015
Received in revised form
26 March 2015
Accepted 13 April 2015
Available online 23 April 2015

Keywords:
Fission fragment spectroscopy
Timing resolution
Artificial diamond
Chemical vapor deposited diamond
Time-of-flight

ABSTRACT

Single-crystal chemical vapor-deposited diamond (sCVD) was investigated for its ability to act as fission-fragment detector. In particular we investigated timing and energy resolution for application in a simultaneous time-of-flight and energy measurement to determine the mass of the detected fission fragment. Previous tests have shown that poly-crystalline chemical vapor deposited (pCVD) diamonds provide sufficient timing resolution, but their poor energy resolution did not allow complete separation between very low-energy fission fragments, α-particles and noise. Our present investigations prove artificial sCVD diamonds to show similar timing resolution as pCVD diamonds close to 100 ps. Improved pulse-height resolution allows the unequivocal separation of fission fragments, and the detection efficiency reaches 100%, but remains with about a few percent behind requirements for fragment-mass identification. With high-speed digital electronics a timing resolution well below 100 ps is possible. However, the strongly varying quality of the presently available diamond material does not allow application on a sufficiently large scale within reasonable investments.

1. Introduction

The study of neutron-rich nuclei is important to reveal the characteristics of nuclear matter far from stability. One question in this context is the evolution of the shell structure at large deformation and increasing neutron excess. One experimental approach to produce nuclei far from stability at a sufficient rate is by means of neutron-induced fission. In this process two fragments are produced with a ratio between the heavy and the light fragment mass ranging from 1 to about 2.3, at least one of them created with a large neutron excess, whose properties may then be investigated spectroscopically.

A fissioning nucleus undergoes a deformation process, either spontaneously or particle-induced, until it disintegrates at the so-called scission point into two more or less deformed fragments. Both fragments share the excess energy, which is not transferred into kinetic energy. This excitation energy, typically of the order of several tens of MeV, is subsequently released through the emission of neutrons and γ-rays at an early stage after scission. By measuring the multiplicity and total energy of the different particles emitted, in conjunction with the corresponding fragments' mass and kinetic energy, we can learn about the mechanism of the nuclear fission process. Those experimental data enter in fission models, which may allow calculating fission characteristics for isotopes not accessible for experiments because of their short lifetime, high radioactivity or small abundance.

In particular, neutron- and photon-induced reactions on actinides are used to study the fission process and to supply the community with fission fragment data relevant for producing the evaluated nuclear data files (cf. Refs. [1–3]). The continuous improvement of the quality of those evaluated nuclear data files is of utmost importance for the successful design of the next generation nuclear reactors [4], contemplated serving for a cleaner, more sustainable and safe energy supply.

The desired observables to be measured in fission are primarily mass, kinetic energy and nuclear charge of both fission fragments as well as the characteristics of emitted prompt neutrons and γ-rays.

A direct way to determine fission fragment masses is to measure both their velocities and kinetic energies. An experimental setup with a flight path of 50 cm and an energy resolution typical for a silicon detector, i.e. 0.3% FWHM, would require measuring the time-of-flight (TOF) between fission source and fragment detector with a timing resolution of the order of 100 ps (FWHM) in order to achieve a mass resolution of $A/\Delta A \approx 100$. Commonly used parallel-plate

* Corresponding author.

http://dx.doi.org/10.1016/j.nima.2015.04.030

avalanche counters as fission-event triggers, however, provide an intrinsic timing resolution of the order of 300–400 ps (FWHM). Micro-channel plate based detectors may be faster by a factor of 2 at least, but are very difficult to operate and sensitive to radiation damage.

Another application, where a good timing resolution in fragment detection matters, is the measurement of prompt fission γ-rays. Since those γ-rays are emitted simultaneously with fission neutrons, the time-of-flight technique is applied to separate both. With the recent availability of fast scintillators made of lanthanide halides (see e.g. Refs. [5,6] and references therein) for prompt γ detection, with a timing resolution for a $LaBr_3$:Ce detector of size 5.0 cm × 5.0 cm (diameter × length) as good as 338 ± 18 ps (FWHM) at optimum energy resolution [7], it is important to achieve a comparable or even better intrinsic timing resolution with the fission-fragment detector.

Furthermore, it would be desirable that the fission fragment detector could provide energy information that could be used for identification of the fission fragments to allow studying the dependence of prompt fission γ-ray emission of mass and energy of the fragments.

Another issue is that, due to the very broad fission-fragment mass and energy distributions in fission, a sufficiently high number of events have to be recorded, especially in measurements where coincidence is required with fission γ-rays or neutrons. It is therefore desirable to have an efficiency as high as possible. A simple and economic way of doing so is to maximize the solid angle by placing the detectors as close as possible to the target. Unfortunately, fission experiments involving actinides have often to deal with very high α activity, fragment emission and intense neutron fields. Thus, the detectors must be very resistant to radiations and have as little mass as possible, so that the neutron background is minimized. The relatively small kinetic energy per nucleon and the high charge number of the fragments also implies very short stopping range in matter, requiring minimum energy loss before the fragments enter the active detector volume. Double Frisch-grid ionization chambers can fulfill all these requirements, but they provide only the energy of both fragments. The fragments' mass is obtained afterwards during data analysis with the help of momentum conservation and the knowledge of the prompt neutron emission. Also, the time resolution of ionization chamber is in the range of 1 ns, limiting the use of this signal for time-of-flight measurements. Therefore, a detector material is needed that can be used as ultra-fast fission trigger with a timing resolution equal to or less than 100 ps, mounted very close to the target and providing sufficiently good energy resolution. One candidate is diamond material, which is presently available made by chemical vapor deposition (CVD). This material in its poly-crystalline form has already proven to be radiation resistant to relativistic heavy ions and to posses excellent timing properties [8,9].

The present work focusses on the possibility of measuring fission-fragment masses with high resolution, including measurements of prompt fission γ-rays and neutrons with high efficiency using single-crystal chemical vapor deposited (sCVD) diamonds.

2. Artificial diamonds for fission-fragment detection

Diamond is an insulator with one of the highest electron–hole drift velocity. Electron–hole pairs created by interaction with charge particles can be collected rapidly and, with appropriate pre-amplifiers, the formed pulse has a rise time faster than 1 ns and a width well below 5 ns, depending on the diamond thickness and the strength of the electric field. These features allow diamond to achieve a timing resolution as good as 29 ps (1σ) in experiments involving heavy ions of very high energy [8]. In the late 1990 and early 2000 years, artificial poly-crystalline diamonds produced by means of chemical vapor deposition became available at sufficiently large size. Combined with diamond's very high resistance to light-charged particles, poly-crystalline chemical vapor deposited diamond (pCVDD) has shown to serve as very efficient detector in beam tracking applications. Since a typical fission experiment takes place in a strong (fast) neutron environment, sometimes in combination with a high α-activity of the target material under investigation, a radiation resistant fission detector is needed. The observed features of diamond makes it a very good candidate for detection of fission fragments.

Relatively affordable and available in large dimensions, pCVDD was already used for the detection of fission fragments [9] and an excellent intrinsic time resolution of 106 ± 21 ps was observed. Unfortunately, due to the poor energy response of pCVDD, especially for the heavier low-energy fragments, a part of the fission fragments was not detected, leading to a significant distortion of the TOF spectrum. The poor energy resolution of pCVDD is caused by the recombination of electrons and holes in the vicinity of defects near grain boundaries. It may be expected that the use of single-crystal chemical vapor deposited diamond (sCVDD) will significantly improve the energy resolution and improve the detection efficiency at low particle energies.

3. Single-crystal diamond

Single-crystal diamonds have a defect density that is significantly reduced in comparison to poly-crystalline diamonds. As a consequence, the charge collection efficiency may reach almost 100%, and an energy resolution as good as 0.4% was measured for α-particles in a selected diamond detector [10]. A detector made from sCVD diamond was also used in a TOF setup and a timing resolution as good as 35 ps was measured for 6 MeV protons and 28 ps for 2 AGeV ^{27}Al [11]. If both timing and energy resolution were that good for the detection of fission fragments, diamond detectors would allow unprecedented mass-resolution in TOF measurements. However, the results previously presented were obtained for very light ions such as protons, α-particles or ions of very high energy.

In contrast, fission-fragment mass distributions range roughly from $A=70$ to $A=170$ with kinetic energies between 2 AMeV and 0.5 AMeV. For fission fragments the energy deposition is occurring in the first few micrometers, which leads to a much higher plasma density than in the event of an impinging light ion at ultra-high kinetic energy. Evidently, the above mentioned properties of sCVD diamond detectors may not be the same. In the following we describe the characterization of sCVD diamond detectors with fission fragments.

We characterized two types of diamond detectors with different specifications and designs. The first three diamond detectors, hereafter called detector A(1) to A(3), consist of 4 pixels of 4.6 × 4.6 × 0.3 mm diamonds each, glued in square configuration on a ceramic PCB board [12]. Faces of the detectors were metallized with a 100 nm thick aluminum coating. The rear side is kept at ground potential and each front side pad was connected through a wire bond to a bias voltage $U=+300$ V. The second detector type (B) has one diamond of similar dimensions as above, but a thickness of 0.15 mm [13]. The recommended bias voltage of $U=+100$ V was applied. The diamond is encapsulated in a RF-shield with an opening of 3 mm diameter. Of two such detectors, one has a 200 nm thick Al (B-Al) and the other a Ti–Pt–Au (B-Au) composite metallization, 470 nm thick. The energy resolution of the sCVD diamond detectors was determined with a ^{241}Am source, emitting α particles with an energy $E_\alpha = 5.49$ MeV, and a ^{252}Cf source emitting both α particles and fission fragments.

The timing resolution was determined with the ^{252}Cf source as described below. Data has been recorded either with analog electronics or two different wave-form digitizers.

4. Energy resolution of single-crystal diamond detectors

4.1. Energy resolution for alpha particles

The energy resolution of the detectors was first estimated with a mixed isotope α source (^{239}Pu, ^{241}Am, and ^{244}Cm). The detector output was amplified with a charge-sensitive (CS) preamplifier MPR1 from Mesytec [14] and shaped by an Ortec 571 [15] spectroscopy amplifier. The shaped signal was then recorded by a Silena 8k ADC [16] at 1 mV/channel. The energy spectrum is shown in Fig. 1. Energy spectra taken with diamond detectors A (3) and B-Al are shown and compared with one obtained with a passivated implanted planar silicon (PIPS) detector (active area 450 mm^2). The energy resolution FWHM/E is found to be 1.28% for detector A(3) and 0.66% for detector B-Al. With the same acquisition chain the silicon detector shows an energy resolution of 0.34%. Apparently, the energy resolution of the present diamond detectors is significantly worse than the best reported value in literature, but representative of what could be achieved in average with single-crystal diamonds so far [17].

The use of a charge sensitive preamplifier significantly improves the signal over noise ratio, but leads to a longer signal rise time of the output signal compared to that of a fast broadband preamplifier. This compromises the achievable timing resolution. In order to benefit from both a very fast rise time of the diamond and a reasonable energy resolution, we investigated the possibility of using a wave-form digitizer with a sufficiently high sampling rate to record the entire trace coming from a fast broadband preamplifier. From the digitized pulse we may then extract pulse height and timing information. Two different wave-form digitizer (WFD) modules were used. The first module was Acqiris DC282 [18] with 4 channels and 10 bit resolution. This board may be used with a sampling speed of 2.0 GS/s, 4.0 GS/s and 8.0 GS/s by using of the interleaving technique. The second WFD module was a two-channel module with 12 bit resolution with sampling rates of 1.8 GS/s and 3.6 GS/s [19]. The average rise time was around 800 ps, significantly faster than attainable with a charge-sensitive preamplifier. As preamplifier we used a current sensitive amplifier, DBA-IV, which has a gain of up to 50 dB and a bandwidth of 2.0 GHz [20].

The energy resolution was determined for all three diamond detectors A with the same mixed nuclide α source that was used with the CS pre-amplifier. The pulse height was obtained by applying a spline function to the trace in order to interpolate between the samples and to reduce the contribution from the noise. This function uses local third order polynomials centered on each sample and was adjusted to match the polynomial of the neighbors in a way that the spline results in a smooth function. The integral of the spline was then calculated between the beginning of the pulse, defined as 10% of the maximum amplitude, and the end of the pulse, again corresponding to 10% of the maximum value. The energy resolution is depicted in the upper part of Fig. 2, obtained with each digitizer and the corresponding sampling rates. An energy resolution of 4% was observed averaged over the three α-particle energies. Increasing the sampling speed from 2 GS/s to 4 GS/s (from 1.8 GS/s to 3.6 GS/s for the SPD digitizer) improved the energy resolution. At low sampling speed the time interval between the points is important, i.e. 500 ps at 2 GS/s. With a pulse as narrow as 4 ns, significant details may be missed. It is then coherent that the increase of sampling speed leads to an improved resolution. However, further increase of the sampling rate increases the bandwidth of the system, causing a lower signal-to-noise ratio, which in turn worsens the energy resolution despite a better pulse sampling. From Fig. 2 one may conclude that a broadband pre-amplifier in connection with a (high-speed) WFD cannot provide an energy resolution as good as a CS preamplifier, here used in an analog setup. Furthermore, by comparing the different pixels of each detector A, the achieved energy resolution may vary by more than 15% as seen in the lower part of Fig. 2. This variation may be attributed to differences in

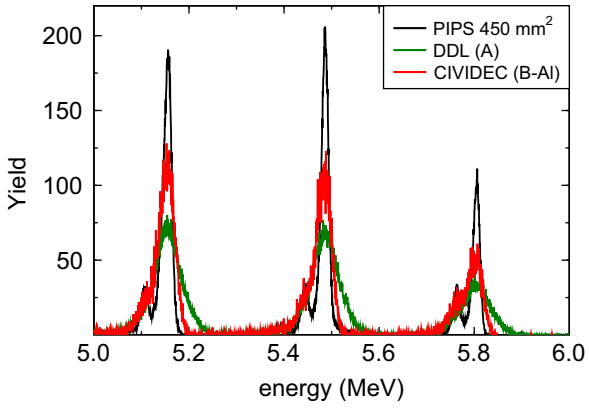

Fig. 1. Energy spectrum of a mixed isotope α source obtained with diamond detectors A(3) (green line) and B-Al (red full line) as well as a silicon detector (black line) for comparison (see text for details). (For interpretation of the references to color in this figure caption, the reader is referred to the web version of this paper.)

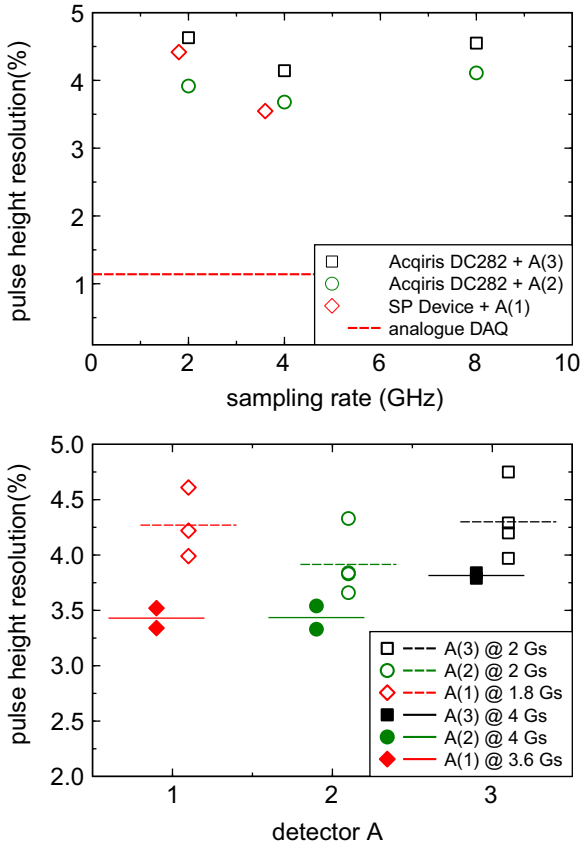

Fig. 2. Energy resolution at $E_\alpha = 5.49$ MeV obtained with measurements with two different wave-form digitizers and various sampling rates (see text for details). The dashed (red) line in the upper panel depicts the corresponding pulse-height (PH) resolution obtained with an analog data acquisition. Full and dashed lines in the lower part give the average PH resolution of each detector and sampling rate. (For interpretation of the references to color in this figure caption, the reader is referred to the web version of this paper.)

diamond quality, because they are all individually grown. Again, a higher sampling rate seems to allow reducing this variation significantly.

4.2. Energy resolution for fission fragments

In the next step the pulse height characteristics for fission fragments were investigated. We used a setup similar to the one described in Ref. [9]. A ^{252}Cf source was mounted practically on top of the first detector, acting as a start detector. A second detector was placed about 90 mm away from the source. During the characterization different combinations of detectors were used. As a consequence, the exact distance between the detectors and the source varied. The source was deposited on a 250 nm thick Ni backing and positioned as close as possible to the detector surface, i.e. at a distance smaller than 1 mm. The californium deposit was on the face opposite to the close detector, meaning that the fragment hitting this detector had to cross the backing. The whole setup was kept in a vacuum chamber at a pressure of less than 2.0×10^{-3} mbar.

We first investigated the detector response in a symmetric setup, where two similar detectors of type A were used. The corresponding energy spectra are shown in Fig. 3. The two spectra, taken at close (upper part) and remote position (lower part), are rather different as depicted by the blue lines. The lower spectrum shows the characteristic double humped structure, associated with heavy and light fission fragments. This distribution is well separated from the α-particle spectrum that can be seen at low pulse height. For the detector located close to the source, in contrast, the spectrum is very different and it is not possible to distinguish the fission-fragments from α-particles. Instead, a broad distribution is observed, extending continuously from high pulse height down to the α region. Due to the very small distance between the detector and the source (0.7 mm), the fragments are detected with a very large angle leading to considerable energy losses in the backing of the source and in the metallization deposit on top of the detector. The immense count rate of this ^{252}Cf source (2000 fissions/s and 60 000 α-decays/s) could also lead to pile-up of fragments with α-particles. The latter effect can be well inferred from the width of the α-peak. Imposing a coincidence condition on the detection of a fission fragment pair in both detectors suppresses the α contribution in the spectrum considerably, as seen from the red curve in the lower part of Fig. 3. Although the impact of energy loss in the backing is now restricted, due to the much narrower angular cone determined through the remote detector, a separation of light and heavy fission fragments is still not possible and the energy of the fragments with the lowest energy is very close to the energy of α particles in the spectrum. This result is comparable to what was previously observed with pCVD diamond detectors [9]. It is important to note here as well that only one of the four diamond pixels on the detector showed an energy response that was sufficient to be used. The three others had slower rise times and significantly lower pulse heights.

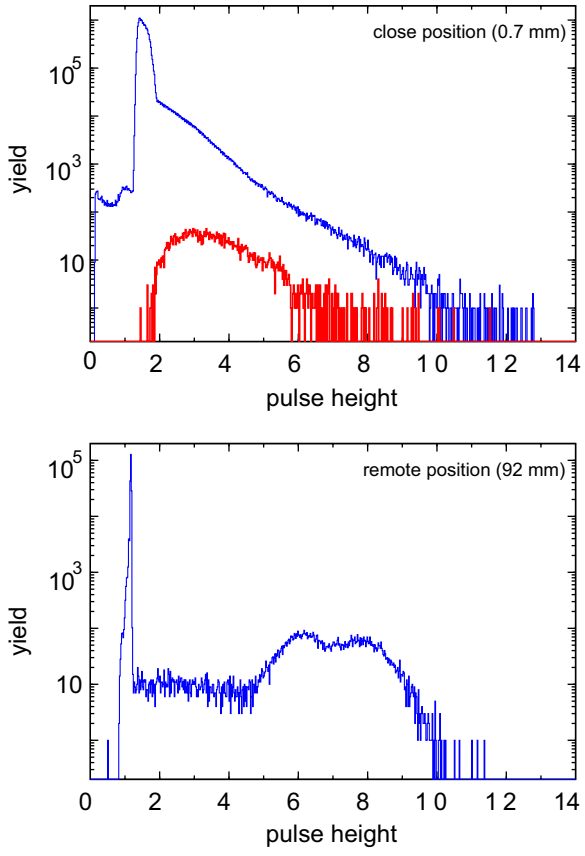

Fig. 3. Fission fragment pulse-height spectra detected with two detectors of type A at two different positions, one close to the ^{252}Cf spontaneous fission source (upper part) and the second (remote, lower part) at a distance of 92 mm. In contrast to the blue curves the red one was obtained with a coincidence condition (see text for details). (For interpretation of the references to color in this figure caption, the reader is referred to the web version of this paper.)

Next, we replaced detector A in close position by the detector B with gold metallization (B-Au). The distance to the source was now about 2 mm due to the RF housing around the diamond detector. Detector A(3) in remote position was left in the setup. The detector in close position was read out by an Ortec 142 charge-sensitive preamplifier [15] and the remote detector was read out by a Caen A1422 charge-sensitive preamplifier [21]. The corresponding kinetic energy spectra were calibrated in MeV with the help of a pulse generator and α-particles from ^{252}Cf and are shown Fig. 4. A coincidence between both fragments was always required. Also, with the help of the TOF information, it was possible to distinguish between the heavy and the light fragment. The corresponding spectra are shown by the red line for the light fragment and the blue line for the heavy fragment. The spectrum for the remote detector, which should be similar to the one in Fig. 3, is significantly modified by the appearance of a tail at lower energies. This difference might be related to the aging of the detector, because almost 10^9 fragments (plus 30 times more α-particles) had hit the detector since the start of the measurement campaign. It can be observed that the pulse height distribution from the detector in close position starts around 15 MeV, i.e. the separation between α particle and fission fragments is fully accomplished, although it is still not possible to see a double-humped distribution. The count rate on the close detector, with the present ^{252}Cf source, was now only about 900 fission fragments and 27 000 α-particles/s.

We finally replaced detector A(3) in remote position by detector B-Al with aluminum coating. The detector with gold coating remained in close position. The black curves in Fig. 5 show the total energy spectrum for ^{252}Cf spontaneous fission with a requirement of a coincidence between the two detectors. The upper part shows the spectrum for the detector in close position. The pulse height distribution has a similar shape as observed in the previous test (see Fig. 4). However, the pulse height dropped by a factor of two. Once more, aging of the detector may explain the drop, because this detector had, in the meantime, suffered from an integral dose of 1.4×10^{10} fission fragments plus 30 times more α-particles. The corresponding energy spectrum of the remote detector is depicted in the lower part of Fig. 5. The count

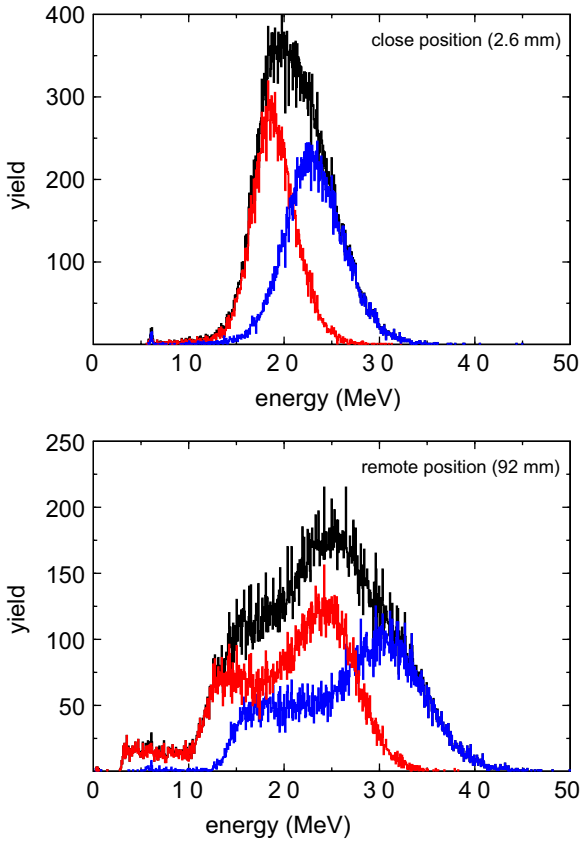

Fig. 4. Fission fragment energy spectrum detected in coincidence by the detector B with gold metallization, B-Au, in close position (upper part) and detector A(3) in remote position (lower part). The black line depicts the total distribution, whereas blue and red lines show the contribution from light and heavy fragments, respectively, separated by their time-of-flight. (For interpretation of the references to color in this figure caption, the reader is referred to the web version of this paper.)

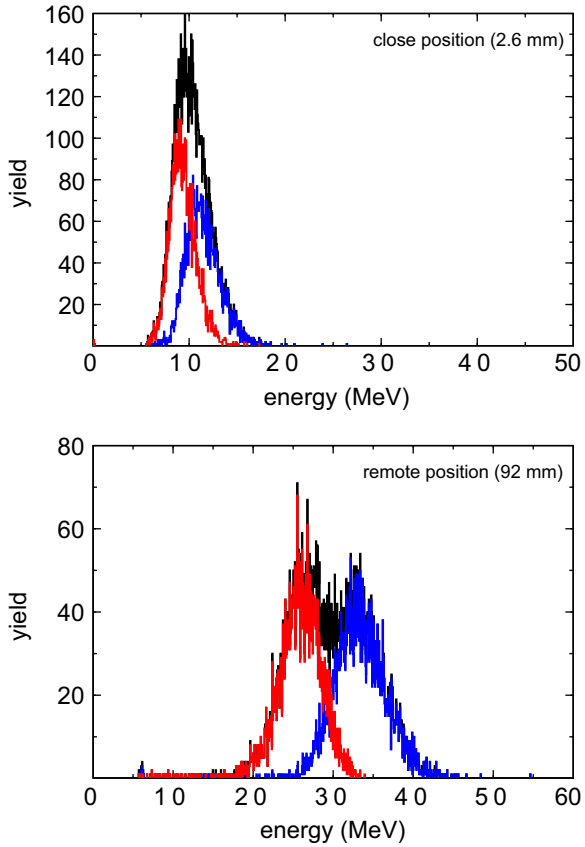

Fig. 5. Fission fragment energy spectrum detected in coincidence by the detector B with gold metallization, B-Au, in close position (upper part) and detector B-Al with aluminum metallization in remote position (lower part). The black line depicts the total distribution, whereas blue and red lines show the contribution from light and heavy fragments, respectively, separated by time-of-flight. (For interpretation of the references to color in this figure caption, the reader is referred to the web version of this paper.)

rate was only around 30 α/s and 1 FF/s. For the first time it was possible to observe a double-humped structure corresponding to light and heavy fission fragments. Still, neither the absolute energy nor the shape of the distribution is close to the requirements for fission-fragment spectroscopy.

At present we can conclude that all sCVD diamond detectors show inadequate energy resolution and suffer from an extensive pulse-height defect (PHD). That the detectors B show a somewhat better performance might be related to edge effects, whereas in the detectors of the A-series the entire diamond surface is active and field distortions at the edge might reduce the charge collection efficiency leading to a deterioration of the energy resolution. B-detectors are sufficiently collimated so that only the central part of the diamond is illuminated. In order to quantify the observed characteristics, we performed Monte Carlo simulations using data for spontaneous fission from Ref. [22]. In a first simulation we assumed an energy resolution of 0.3% and no PHD. The corresponding energy spectrum is shown in the upper part of Fig. 6. In order to reproduce the measured pulse height distribution observed in close position (cf. the upper part of Fig. 4), it was necessary to assume an energy resolution of only 7% and a PHD as large as 75%. These two values are of course different for the different detectors and vary as a function of the count rate as well as of the absorbed dose. In any case, the detected pulse height never exceeds about 30% of what is expected for fission fragments.

A possible explanation for the observed limitations could be found by recombination, charge trapping or depolarization of the crystal. This could be overcome by an increase of the field strength across the crystal. Increasing the bias voltage showed little improvement. However, the maximum bias, recommended by the manufacturer, i.e. $U = +150$ V, could not be applied to the detector.

5. Timing resolution of single-crystal diamond detectors

For the investigation of the timing characteristics of our diamond detectors we need collinear emitted particles, e.g fission fragments measured in coincidence. The setup is very similar to the one described in Ref. [9].

First, we used two detectors of type A. The distance from the fission sample to the remote detector was again around 95 mm and to the close detector less than 1 mm. In order to achieve optimum timing resolution, current-sensitive preamplifiers (DBA-IV [20]) were used again. In order to minimize distortion of the signal between the feedthroughs on the chamber and the pre-amplifier, cables with high shielding and a bandwidth as high as 18 GHz were used. In these conditions an average rise time around 800 ps was observed for signals associated with fission fragments. Timing information was obtained with a constant fraction discriminator (CFD) Ortec 934 [15]. The time spectrum was recorded with a time-to-amplitude converter (TAC) and digitized with an ADC (cf. Section 4.1). The delayed signal

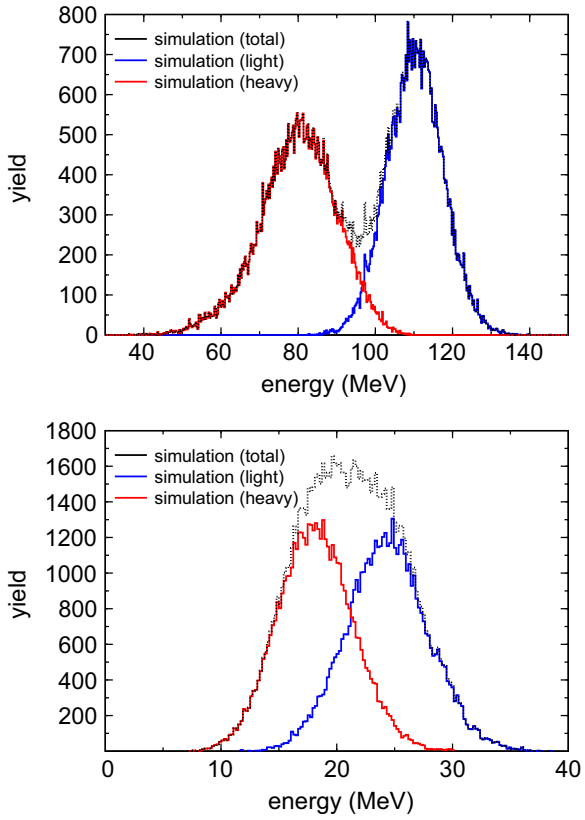

Fig. 6. Simulation of the energy distribution considering an energy resolution of 0.3% and zero pulse-height defect (PHD) (upper part) and with an energy resolution of 7% and a PHD of 75% (lower part). The black (dotted) line depicts the total distribution, whereas blue and red lines show the contribution from light and heavy fragments, respectively. (For interpretation of the references to color in this figure caption, the reader is referred to the web version of this paper.)

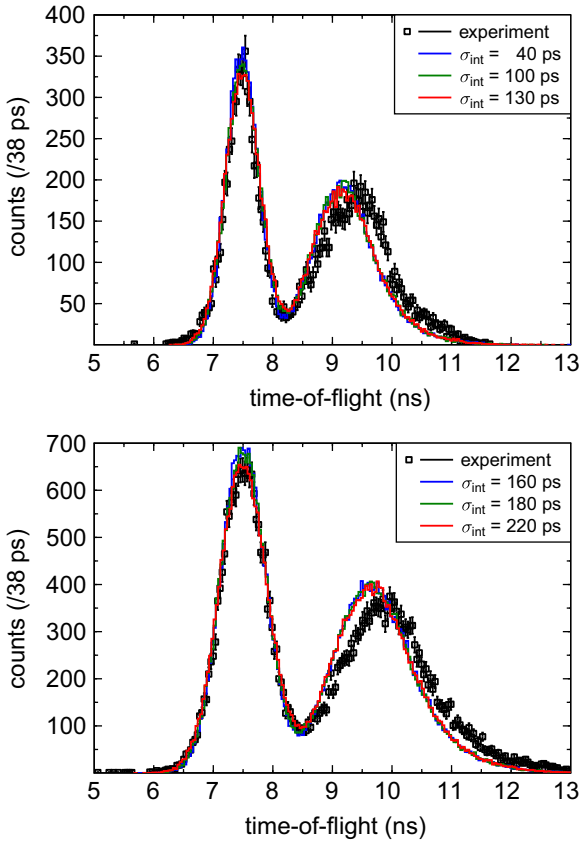

Fig. 7. Time-of-flight distribution of fission fragments of ^{252}Cf compared with Monte-Carlo simulations for a symmetric setup consisting of two detectors of type A (top panel) and for a setup, where the close detector was replaced by the detector B-Al (lower panel). In both figures Monte-Carlo simulations with different values for the intrinsic timing resolution, that fit the experimental data best, are depicted with full colored lines (see text for details). (For interpretation of the references to color in this figure caption, the reader is referred to the web version of this paper.)

from the remote detector served as start signal, the signal of the close detector as stop signal. The time jitter introduced in the stop detector by the velocity distribution of the fission fragments was well below 40 ps FWHM, but the effect is properly taken into account in the TOF simulations.

The time spectrum was calibrated with the help of a time calibrator. This procedure, due to the uncertainty coming from the propagation delay in the electronic chain, could only provide us with the slope of the calibration. The absolute TOF was, therefore, adjusted to better reproduce the time spectrum produced with the Monte Carlo simulation used to extract the timing resolution.

Since fission fragments show a broad distribution in mass and kinetic energy, which translates into a broad variation of fragment velocities, it is not possible to infer the timing resolution based on the width of the measured TOF distribution. The timing resolution must be evaluated by comparing the experimental TOF spectrum with Monte Carlo simulations, a technique already applied in Ref. [9]. The simulations were performed with the help of experimental data for the total kinetic energy and mass yield distribution for the spontaneous fission of ^{252}Cf [22]. With these quantities the velocity of both fragments was calculated. The energy of the fragment crossing the source backing was corrected for energy loss according to Ref. [23]. The TOF of both fragments was then calculated and convoluted with a Gaussian distribution with width σ_{int}, representing the intrinsic timing resolution of each detector. Finally, the TOF of the fragment that is detected close to the source is subtracted from that of the other fragment until best reproduction of the measured TOF distribution is achieved.

Considering the source strength and age of our ^{252}Cf source, we assumed the active layer at a depth of 50 nm in the support backing, as a result of recoil. However, this is a first-order approximation, which neglects the fact that implantation due to recoil leads to a distribution of californium atoms in the support. This results in an increasing energy loss for increasing fragment masses (with correspondingly decreasing average kinetic energy). Since the distribution is not known a priori, we did not include a distributed source in our simulations. The result is that we have a perfect description of the light fragment peak (low TOF values) beyond the minimum of the distribution and increasing deviation for higher TOF values.

The top part of Fig. 7 depicts the TOF distribution measured with two type-A detectors (black symbols). The error bars include statistical uncertainties only. Three simulations are shown, assuming three different intrinsic timing resolutions of the diamond detectors. The simulation assuming a timing resolution $\sigma_{int} = 100^{+30}_{-60}$ ps (green full line) reproduces the experimental data with the lowest χ^2. The uncertainties on σ_{int} are estimated from those simulations, which describes the data within the upper and lower experimental uncertainties. This is a value that confirms the timing characteristics already found with pCVD diamond detectors [9]. The corresponding peak-to-valley ratio of the distribution, P/V, is about 11. Since the Monte-Carlo simulations are based on fission-fragment data obtained with a double-energy experiment, a realistic estimate of the uncertainty at such small values of σ_{int} is not possible.

Next, we replaced the close detector with a detector of type B (B-Al) close to the source. Due to the RF-housing, the distance between diamond and fission source is again increased to 2.6 mm. The corresponding TOF spectrum is shown in the lower part of Fig. 7, where the black symbols denote the experimental points. Again, the errors bars only include statistical uncertainties. The values are

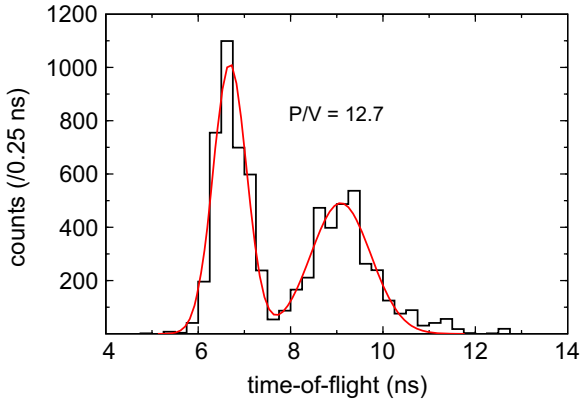

Fig. 8. Time-of-flight distribution of fission fragments from the spontaneous fission of ^{252}Cf obtained with two detectors of type A recorded with a two-channel waveform digitizer [19] at sampling rate of 3.6 Gs/s and 12 bit resolution (histogram). The full (red) line is a simple fit to the experimental data to extract the peak-to-valley ratio, *P*/*V*, assuming a Gaussian distribution for both light and heavy fragments. (For interpretation of the references to color in this figure caption, the reader is referred to the web version of this paper.)

compared with the results from Monte Carlo simulations. Three simulations, with $\sigma_{int}=160$, 180 and 220 ps, are shown as lines in different colors. The simulation that gave the best reproduction of the experimental data according to the corresponding χ^2, is the one with a timing resolution $\sigma_{int}=180^{+40}_{-20}$ ps. Here, an uncertainty of the order of ± 20 ps is estimated from the distribution of χ^2-values.

One possible explanation for the worse timing resolution is the smaller thickness of detector B, which is only 150 μm in comparison to 300 μm for the type-A detector. A difference in thickness increases the capacitance of the detector. This, in turn, leads to a slower rise-time and, thus, to a diminished timing resolution. Also, the lower bias voltage applied to detector B, i.e. 0.67 V/μm, in accordance with the manufacturer specification, might contribute to the significant deterioration. Also a contribution from the different metallization, leading to inhomogeneous electric fields, is possible, but could not be investigated quantitatively.

Complementary to the tests with digitizers reported in Section 4.1, we used the SPDevice digitizer [19] at 3.6 GS/s. Those tests were again performed with a symmetric setup consisting of two type-A detectors in close and remote position. The digitizer has two synchronized channels, which were fed with the corresponding output signals of each of the detectors. The timing information was extracted by applying a digital constant fraction discriminator algorithm to the digitized signal. Each signal was first fitted by a third-order spline function and then copied, delayed by 900 ps and inverted, while the original was multiplied by a factor of 0.2. The zero-crossing of the summed signal was used as the time reference for each signal. The difference between the two different time references is a measure of the TOF. The resulting TOF-spectrum is shown in Fig. 8. In comparison to the other distributions measured with CFD, TAC and ADC, the *P*/*V* ratio appears to be very good. Unfortunately, the relatively low number of events required a large binning and did not allow a comparison with Monte-Carlo simulations. With the aid of a fit with Gaussians to the TOF distribution, we determined *P*/*V* to 12.7, indicating an intrinsic timing resolution considerably better than 100 ps.

Of course, despite this impressive result, we have to stress the fact that digitizers with both a high sampling rate and a large number of bits are mandatory to obtain timing resolutions well below 100 ps, even with diamond detectors. Apart from the fact that synchronization of digitizer boards is a challenge, the relatively high price per channel may severely limit the application of this technique in a large scale experiment.

6. Conclusion

Diamond material has proven to be very useful in experiments, where a timing precision in the sub-100 ps range is required, especially when broad-band pre-amplifiers are combined with waveform digitization. In addition, diamond material stands very high radiation doses from heavy ionizing particles, like e.g. around 10^9 fission fragments plus 3×10^{10} α-particles. Thus, radiation resistance is sufficient for all typical correlation experiments between fission fragments and promptly emitted γ-rays or neutrons, where precise timing is crucial. This is valid for the previously investigated polycrystalline as well as for the presently studied single-crystal diamonds, manufactured by means of chemical vapor deposition. Thanks to the improved pulse-height resolution in sCVD diamond, detection efficiency now reaches 100%.

However, our investigation shows also that the present pulse-height resolution of at best a few percent, observed at only relatively low count rates of a few fragments/second, and the observed pulse-height defect, do not allow fission-fragment spectrometry yet. Up to now, further limitation is caused by the largely varying diamond quality. Only about 25% of the material investigated in our study showed sufficient quality to provide the presented characteristics to the experimentalists. This is a fraction, which makes large scale application in nuclear physics experiment very costly.

Acknowledgment

One of the authors (M.O.F.) is indebted to the European Commission for providing a Post-doc fellowship at the EC Joint Research Centre IRMM, during which this work was carried out.

References

[1] ⟨https://www.oecd-nea.org/dbdata/jeff⟩.
[2] ⟨https://www-nds.iaea.org/exfor/endf.htm⟩.
[3] ⟨http://wwwndc.jaea.go.jp/jendl/j40/j40.html⟩.
[4] G. Rimpault, in: P. Rullhusen (Ed.), Nuclear Data Needs for Generation IV, World Scientific, Antwerp, 2006, p. 46.
[5] A. Oberstedt, S. Oberstedt, R. Billnert, W. Geerts, F.-J. Hambsch, J. Karlsson, Nuclear Instruments and Methods in Physics Research Section A 668 (2012) 14.
[6] R. Billnert, S. Oberstedt, E. Andreotti, M. Hult, G. Marissens, A. Oberstedt, Nuclear Instruments and Methods in Physics Research Section A 647 (2011) 94.
[7] A. Oberstedt, R. Billnert, S. Oberstedt, Nuclear Instruments and Methods in Physics Research Section A 708 (2013) 7.
[8] E. Berdermann, K. Blasche, P. Moritz, H. Stelzer, B. Voss, Diamond and Related Materials 10 (2001) 1770.
[9] S. Oberstedt, R. Borcea, T. Brys, T. Gamboni, W. Geerts, F.-J. Hambsch, A. Oberstedt, M. Vidali, Nuclear Instruments and Methods in Physics Research Section A 714 (2013) 31.
[10] M. Pomorski, E. Berdermann, C. Ciobanu, M. Martemiyanov, P. Moritz, M. Rebisz, B. Marczewska, Physica Status Solidi A 202 (2005) 2199.
[11] E. Berdermann, M. Pomorski, W. de Boer, M. Ciobanu, S. Dunst, C. Grah, M. Kiš, W. Koenig, W. Lange, W. Lohmann, R. Lovričić, P. Moritz, J. Morse, S. Mueller, A. Pucci, M. Schreck, S. Rahman, S. Träger, M. Träger, Diamond and Related Materials 19 (2010) 258.
[12] Diamond Detectors Limited (now E6), ⟨http://www.e6cvd.com⟩.
[13] ⟨http://www.cividec.at⟩.
[14] ⟨http://www.mesytec.com/datasheets/MPR-1.pdf⟩.
[15] ⟨http://www.ortec-online/Products-Solutions/index.aspx⟩.
[16] See e.g. ⟨http://alga.pnpi.spb.ru/gagarski/scr1/saved/old_alga/home/gagarski/CatalogoWeb.pdf⟩.
[17] M. Pomorski, E. Berdermann, A. Caragheorgheopol, M. Ciobanu, M. Kiš, A. Martemiyanov, C. Nebel, P. Moritz, Physica Status Solidi A 203 (2006) 3152.
[18] ⟨http://www.keysight.com/en/pd-1184897-pn-U1065A/acqiris-10-bit-high-speed-cpci-digitizers?&cc=BElc=dut⟩.
[19] ⟨http://spdevices.com/index.php/products/digitizer-product-overview⟩.
[20] P. Moritz, E. Berdermann, K. Blasche, H. Stelzer, B. Voss, Diamond and Related Materials 10 (2001) 1765.
[21] ⟨http://www.caen.it/csite/⟩.
[22] F.-J. Hambsch, S. Oberstedt, Nuclear Physics A 617 (1997) 347.
[23] L. Northcliffe, R. Shilling, Atomic Data and Nuclear Data Tables 7 (1970) 233.